

Machine learning-based conditional mean filter: a generalization of the ensemble Kalman filter for nonlinear data assimilation

Truong-Vinh Hoang*, Sebastian Krumscheid*, Hermann G. Matthies†, and Raúl Tempone *‡

Abstract. *Filtering* is a data assimilation technique that performs the sequential inference of dynamical systems states from noisy observations. Herein, we propose a machine learning-based ensemble conditional mean filter (ML-EnCMF) for tracking possibly high-dimensional non-Gaussian state models with nonlinear dynamics based on sparse observations. The proposed filtering method is developed based on the conditional expectation and numerically implemented using machine learning (ML) techniques combined with the ensemble method. The contribution of this work is twofold. First, we demonstrate that the ensembles assimilated using the ensemble conditional mean filter (EnCMF) provide an unbiased estimator of the Bayesian posterior mean, and their variance matches the expected conditional variance. Second, we implement the EnCMF using artificial neural networks, which have a significant advantage in representing nonlinear functions over high-dimensional domains such as the conditional mean. Finally, we demonstrate the effectiveness of the ML-EnCMF for tracking the states of Lorenz-63 and Lorenz-96 systems under the chaotic regime. Numerical results show that the ML-EnCMF outperforms the ensemble Kalman filter.

Key words. Artificial neural network, nonlinear filter, inverse problem, conditional expectation, weather forecast

AMS subject classifications. 62M45, 62M20, 93E11, 65C20, 6008,

1. Introduction. Data assimilation combines numerical models and observations of a dynamical system to infer its states. This approach of integrating data into dynamical models is essential in different applications, e.g., numerical weather prediction, environmental forecasting, and digital twins [4, 19, 29, 31, 16, 5, 28]. Filtering is a sequential data assimilation technique usually comprising two steps: a) forecasting of the states using the numerical models up to an observation event (forecast step) and b) updating of the forecasts by conditioning on new observations (analysis step). Ideally, the analysis step should be performed using Bayes' rule, where the forecasting states are encoded as a prior distribution, and the updated states are obtained as the Bayesian posterior. The Bayesian filtering problem has a closed-form solution for linear-Gaussian systems, i.e., the well-known Kalman filter (KF) [17, 12]. However, it is computationally difficult to accurately represent the posterior distribution in the case of nonlinear systems, even prohibitive for high-dimensional state spaces [2, 22, 30].

The ensemble Kalman filter (EnKF) is an extension of the KF for nonlinear settings [16, 12, 20, 15]. The EnKF uses an ensemble to approximate the forecast distribution which is then updated by applying the KF formulation to each ensemble member. Because the EnKF uses a linear updating formulation, the assimilated ensemble mean is generally biased with respect to the Bayesian posterior mean. For nonlinear dynamical systems with sparse observations, the EnKF shows poor performance in predicting the system states owing to its

*Chair of Mathematics for Uncertainty Quantification, RWTH Aachen University, Germany (hoang@uq.rwth-aachen.de, krumscheid@uq.rwth-aachen.de, tempone@uq.rwth-aachen.de).

†Technische Universität Braunschweig, Germany (h.matthies@tu-bs.de).

‡Computer, Electrical and Mathematical Sciences and Engineering, KAUST.

linear filtering map [22, 30]. Lei and Bickel [22] improved the EnKF using a moment matching method to enforce that the mean and variance of the assimilated ensemble match those of the posterior distribution. Spantini et al. [30] recently developed an ensemble filtering technique using transport maps to construct a generator for the joint probability of forecast states and observations. These techniques require significant computational resources after acquiring observation data. Alternatively, in the EnKF, the Kalman gain, which is the component requiring the most computational resources for approximation, is estimated before acquiring observation data.

A natural extension of the EnKF is the EnCMF, which is developed based on the conditional mean (CM) [27]. The EnCMF harnesses the advantage of the conditional expectation in characterizing the underlying conditional distribution and ultimately improves the approximation performance of the assimilated ensemble for the conditional distribution. Compared with the *ideal* Bayesian filter, the assimilated ensemble of the EnCMF does not follow the posterior distribution [11]; however, its ensemble mean is unbiased with respect to the posterior mean [27, 32]. While the former is a shared property between EnCMF and EnKF, the latter is a particular advantage of the EnCMF.

For the practical implementation of the EnCMF, knowledge regarding the CM or accurate numerical approximation is required. It is significantly difficult to approximate the CM in non-linear data assimilation problems with high-dimensional state vectors. Thus, state-of-the-art research in this direction (e.g., [27, 20]) employs only linear approximations for the CM. The present work focuses on this challenge. We aim to develop a nonlinear approximation for the CM that can be straightforwardly integrated with the well-known EnKF.

The contribution of this work is twofold. First, we demonstrate that the ensembles assimilated using the EnCMF provide an unbiased estimator of the Bayesian posterior mean; moreover, their variance matches with the expected conditional variance. Second, we implement the EnCMF using artificial neural networks (ANNs) to approximate the conditional expectation. That proposed ML-EnCMF harnesses advantages of ANN in approximating complex functions over high-dimensional spaces, along with its reusability and the advanced hardware technologies designed for ANNs [7, 14]. Several studies that apply ML techniques in data assimilation have been conducted in the literature, e.g., [1, 7, 8, 13]. To the best of the authors' knowledge, most work in this direction centers on developing efficient numerical methods for performing the forecast step, e.g., the use of ML-based surrogate models for dynamical systems. In the present study, we focus on the analysis step, which is a natural continuation of these developments. In particular, our method can be combined with existing approaches to further improve the filtering performance.

In this work, we approximate the CM using its linear approximation, which is obtained based on the (En)KF analysis, combined with an ANN to represent the CM nonlinearity. With this combination, the proposed ML-EnCMF becomes a natural nonlinear extension of the EnKF. Such a combination also improves the robustness of the EnCMF because the EnKF exhibits good performance for data assimilation problems with *closely* linear dynamical models [12].

An important motivation for using the CM in our filter is its particular geometrical interpretation, which describes it as an orthogonal projection of the forecast state RV onto the σ -algebra (i.e., the *information*) of RVs generated by the forecast observation RV [6]. Based

on the orthogonal projection property, we train the ANN using the mean squared error (MSE) loss, which is widely used for ML applications. In an ensemble filter, such as the EnKF and the proposed ML-EnCMF, the forecast ensembles of states and observations are evaluated during the forecast step. Owing to their availability, these forecast ensembles are used as training data to estimate the loss function. Approximating the CM using small-sized ensembles can lead to overfitting. To address with this problem, in addition to the regularization techniques, we use the variance reduction method to reduce statistical errors when approximating the MSE. Finally, we perform a model selection procedure to verify the performance gain obtained using the ML-EnCMF compared with the EnKF.

The reminder of this paper is organized as follows. In Sec. 2, we summarize the KF, its ensemble version, and the Bayesian filter. In Sec. 3, the theoretical property of the EnCMF are discussed. In Sec. 4, the ML-EnCMF is presented. In Sec. 5, the performance of the ML-EnCMF implemented for tracking the Lorenz systems is analyzed. Finally, in Sec. 6, conclusions and future research directions are discussed.

2. Filtering method. Data assimilation techniques seek an optimal forecast of the dynamical system states by combining modeling predictions with observations under the presence of uncertainty. In this section, we present the framework of the filtering approach for data assimilation; in particular, the linear filters are discussed to present their advantages and disadvantages. The detailed theoretical results on filtering techniques can be found in the literature [4, 12, 19].

Let $(\Omega, \mathcal{A}, \mathbb{P})$ be a probability space. We assume that the dynamical system is a random ordinary differential equation (RODE), and the observation model belongs to the additive-noise class:

$$(2.1) \quad \begin{aligned} \frac{d}{dt}Q(t, \omega) &= f(t, Q(t, \omega)) \quad \text{for } t \in (0, T], \quad Q(t=0) = Q_0, \\ Y_k(\omega) &= h(t, Q(t_k, \omega)) + \Xi_k(\omega), \quad 0 < t_1 < t_2, \dots, t_K < T, \end{aligned}$$

where $Q(t)$ is the \mathbb{R}^n -valued RVs of the system states at time t , f is a known operator that can be deterministic or stochastic, Y_k and Ξ_k are the \mathbb{R}^m -valued RVs of the observations and measurement errors, respectively, and $h : \mathbb{R}^n \rightarrow \mathbb{R}^m$ is a known observation map. We assume that the measurement error RVs Ξ_k , with $k = 1, \dots, K$, are statistically independent, and the random process $Q(t)$ satisfies the Markov property. Additionally, the distributions of the RVs $Q(t)$, Ξ_k , and Y_k are assumed absolutely continuous, i.e., their densities exist.

The distribution of the RV $Q(t)$ is interpreted as an uncertainty model of the actual states denoted as $\mathbf{q}^{\text{true}}(t)$. In practice, the observations can be spatiotemporally sparse. Owing to the limitations of operational costs and technical capacity, only some members of the state vector are observable, and the observation time intervals, $t_k - t_{k-1}$, may be relatively large compared with the time step in the integration scheme used to solve the RODE.

Let $\hat{\mathbf{y}}_k \in \mathbb{R}^m$ be the observation data observed at time t_k . We denote the set of observation data up to time t_k as $\mathcal{Y}_k = \{\hat{\mathbf{y}}_1, \dots, \hat{\mathbf{y}}_k\}$. Let Q_k , with $k = 0, \dots, K$, be RVs defined as $Q_k \equiv Q(t_k)$. An accurate representation of the distribution of the conditional RV $Q_k|_{\mathcal{Y}_k}$ is not feasible for high-dimensional state dynamical systems. Based on the assumptions that $Q(t)$ is a Markov process and the measurement error RVs are statistically independent, the

distribution of the conditional RV $Q_k|_{\mathcal{Y}_k}$ can be sequentially approximated, as shown in the literature [12, Chapter 7].

The filtering procedure from time t_{k-1} to t_k usually comprises of two steps: a prediction step, where the conditional density $\pi_{Q_{k-1}|\mathcal{Y}_{k-1}}$ obtained from the previous assimilation step is transformed to the forecast density $\pi_{Q_k|\mathcal{Y}_{k-1}}$ using the RODE in Eq. (2.1), and an analysis step, where *ideally*, Bayes' rule is used to map $\pi_{Q_k|\mathcal{Y}_{k-1}}$ to $\pi_{Q_k|\mathcal{Y}_k}$. To present this procedure in detail, let Q_{k-1}^a be the *assimilated* RV at time step t_{k-1} , in other words, Q_{k-1}^a has a density function identical to $\pi_{Q_{k-1}|\mathcal{Y}_{k-1}}$. The *forecast* RVs Q_k^f and Y_k^f of the states and observations, respectively, at t_k are evaluated as follows:

$$(2.2a) \quad Q_k^f = Q_{k-1}^a + \int_{t_{k-1}}^{t_k} f(t, Q^s(t)) dt \equiv M_k(Q_k^a),$$

$$(2.2b) \quad Y_k^f = h(Q_k^f) + \Xi_k,$$

where $Q^s(t)$ solves

$$\frac{d}{dt} Q^s(t, \omega) = f(t, Q^s(t, \omega)) \quad \text{for } t \in (t_{k-1}, t_k], \quad Q^s(t_{k-1}) = Q_{k-1}^a.$$

To simplify the notation, we represent the time evolution model that maps the state from t_{k-1} to t_k as M_k (Eq. (2.2a)). From Eq. (2.2a), we obtain $Q_k^f = Q_k|_{\mathcal{Y}_{k-1}}$. The independent assumption of RVs Ξ_k yields the following result $\pi_{Q_k|\mathcal{Y}_k} = \pi_{Q_k^f|\hat{\mathbf{y}}_k}$. Hence, the conditional density $\pi_{Q_k|\mathcal{Y}_k}$ can be obtained by conditioning the density of the forecast RV Q_k^f with the measurement data $\hat{\mathbf{y}}_k$. Let $\pi_{Q_k^f, Y_k^f}$ be the joint density of Q_k^f and Y_k^f , the density of the conditional RV $Q_k^f|_{Y_k^f}$ is obtained as

$$(2.3) \quad \pi_{Q_k^f|Y_k^f}(\mathbf{q}|\mathbf{y}) = \frac{\pi_{Q_k^f, Y_k^f}(\mathbf{q}, \mathbf{y})}{\pi_{Y_k^f}(\mathbf{y})},$$

provided that it is well defined. The density $\pi_{Q_k^f|Y_k^f}(\cdot|\hat{\mathbf{y}}_k)$ is also known as the Bayesian posterior density of RV Q^f given the observation data $\hat{\mathbf{y}}_k$, which can be used to approximate the assimilated RV $Q_k^a \sim \pi_{Q_k^f|\hat{\mathbf{y}}_k}$.

The posterior density $\pi_{Q_k^f|Y_k^f}(\cdot|\hat{\mathbf{y}}_k)$ is usually intractable for high-dimensional state vectors. The Markov chain Monte Carlo method often used for sampling such posterior distributions is time-consuming and requires knowledge of the RV Q_k^f density. To address that issue, the filtering approach considered herein seeks a map \mathcal{T}_k that approximates the assimilated RV Q_k^a using the available information encoded in the RVs Q_k^f and Y_k^f and the measurement data $\hat{\mathbf{y}}_k$, namely

$$(2.4) \quad Q_k^a = \mathcal{T}_k(Q_k^f, Y_k^f, \hat{\mathbf{y}}_k).$$

The filtering map \mathcal{T}_k in Eq. (2.4) is usually designed such that the RV Q_k^a accurately represents the posterior density $\pi_{Q_k^f|Y_k^f}(\cdot|\hat{\mathbf{y}}_k)$, while \mathcal{T}_k remains simple to identify and approximate.

A solution for \mathcal{T}_k can be obtained using the Rosenblatt transformation (e.g., in [30]), which requires an approximation of the cumulative distribution function (cdf) of the conditional RV $Q_k^f|_{\hat{\mathbf{y}}_k}$ and its inverse. This theoretical result confirms the existence of the map \mathcal{T}_k . However, approximating the Rosenblatt transformation can be challenging, particularly when enforcing the monotonic property of the map. The present work considers another approach for approximating the map \mathcal{T}_k using conditional expectation.

Data assimilation problems are commonly classified into two categories: *linear-Gaussian setting* and *nonlinear setting*. In the former setting, the maps M_k and h are linear, and the RVs Q_0 and Ξ_k are Gaussian. Alternatively, the latter setting abandons these assumptions. For the linear-Gaussian setting, the filtering map \mathcal{T}_k stated in Eq. (2.4) is linear and exhibits a closed-form. This present work mainly focuses on approximating the map \mathcal{T}_k for the nonlinear setting. The KF and its ensemble version (EnKF) are summarized below. It is noteworthy that these filters use an identical linear filtering map \mathcal{T}_k .

Kalman filter. In the linear-Gaussian setting, the RVs Q_k^f and Y_k^f are considered Gaussian. Consequently, the conditional density stated in Eq. (2.3) is simplified to a normal distribution density. Let $h(\mathbf{q}) = \mathbf{H}\mathbf{q}$, where $\mathbf{H} \in \mathbb{R}^{m \times n}$. The closed-form of the RV Q_k^a , whose probability density is identical to that of the Bayesian posterior [17], is expressed as follows:

$$(2.5a) \quad Q_k^a = Q_k^f + \mathbf{K}_k^l (\hat{\mathbf{y}}_k - Y_k^f),$$

$$(2.5b) \quad \mathbf{K}_k^l = \mathbf{H}^\top \boldsymbol{\Sigma}_{Q_k^f} (\boldsymbol{\Sigma}_{\Xi_k} + \mathbf{H}^\top \boldsymbol{\Sigma}_{Q_k^f} \mathbf{H})^{-1},$$

where Q_k^f is evaluated using the model M_k that is assumed to be linear, \mathbf{K}_k^l is the Kalman gain, and $\boldsymbol{\Sigma}_{Q_k^f}$ and $\boldsymbol{\Sigma}_{\Xi_k}$ are the covariance matrices of the RVs Q_k^f and Ξ_k , respectively. The transformation in Eq. (2.5a) is a linear version of the map \mathcal{T}_k (Eq. (2.4)). In the linear-Gaussian setting, the RV Q^a obtained using Eq. (2.5a) is a Gaussian RV, hence, fully characterized by its mean and covariance. From Eq. (2.5a), the formulations for updating these statistical moments can be straightforwardly derived, known as the KF [17].

Ensemble Kalman filter. The EnKF is an ensemble implementation of the KF for dealing with nonlinear dynamical systems, in which the forecast and assimilated RVs are represented using the ensembles of their samples, thereby allowing the approximation of non-Gaussian distributions [12]. However, the EnKF applicability still requires a linear observation map. Let $\{\mathbf{q}_{k-1}^{a(1)}, \dots, \mathbf{q}_{k-1}^{a(N)}\}$ be the N -sample ensemble of the RV Q_{k-1}^a . The ensembles $\{\mathbf{q}_k^{f(1)}, \dots, \mathbf{q}_k^{f(N)}\}$ and $\{\mathbf{y}_k^{f(1)}, \dots, \mathbf{y}_k^{f(N)}\}$ of the RVs Q_k^f and Y_k^f , respectively, are obtained as

$$(2.6) \quad \begin{aligned} \mathbf{q}_k^{f(i)} &= M_k(\mathbf{q}_{k-1}^{a(i)}), \quad i = 1, \dots, N, \\ \mathbf{y}_k^{f(i)} &= h(\mathbf{q}_k^{f(i)}) + \boldsymbol{\xi}_k^{(i)}, \quad i = 1, \dots, N, \end{aligned}$$

where $\boldsymbol{\xi}_k^{(i)}$ denotes the independent and identically distributed (i.i.d.) samples of Ξ_k . For the analysis step, we first estimate the mean $\bar{\mathbf{q}}_k^f$ and the covariance matrix $\boldsymbol{\Sigma}_{Q_k^f}$ of the RV Q_k^f

using the forecast ensembles:

$$(2.7) \quad \begin{aligned} \bar{\mathbf{q}}_k^f &\approx \frac{1}{N} \sum_{i=1}^N \mathbf{q}_k^{f(i)}, \\ \boldsymbol{\Sigma}_{Q_k^f} &\approx \frac{1}{N} \sum_{i=1}^N \left(\mathbf{q}_k^{f(i)} - \bar{\mathbf{q}}_k^f \right) \left(\mathbf{q}_k^{f(i)} - \bar{\mathbf{q}}_k^f \right)^\top. \end{aligned}$$

The obtained covariance matrix is then used to compute the Kalman gain by evaluating Eq. (2.5b). Subsequently, the EnKF uses the linear filtering map of the KF, as expressed in Eq. (2.5a), and employs the ensemble technique to approximate the assimilated ensemble:

$$(2.8) \quad \mathbf{q}_k^{a(i)} = \mathbf{q}_k^{f(i)} + \mathbf{K}_k^l (\hat{\mathbf{y}}_k - \mathbf{y}_k^{f(i)}), \quad i = 1, \dots, N,$$

where $\{\mathbf{q}_k^{a(1)}, \dots, \mathbf{q}_k^{a(N)}\}$ is the assimilated ensemble representing the RV Q_k^a . Algorithm 2.1 presents a pseudo algorithm of the EnKF.

Algorithm 2.1 EnKF algorithm for performing assimilation at time t_k .

Require: The assimilated ensemble obtained from the assimilation step performed at t_{k-1} $\{\mathbf{q}_{k-1}^{a(1)}, \dots, \mathbf{q}_{k-1}^{a(N)}\}$, the observation data $\hat{\mathbf{y}}_k$, and the covariance matrix of RV Ξ_k .

Forecast:

1: Evaluate the forecast ensembles $\{\mathbf{q}_k^{f(1)}, \dots, \mathbf{q}_k^{f(N)}\}$ and $\{\mathbf{y}_k^{f(1)}, \dots, \mathbf{y}_k^{f(N)}\}$ \triangleright Eq. (2.6).

Analysis:

2: Estimate the covariance matrix $\boldsymbol{\Sigma}_{Q_k^f}$ of the forecast RV Q_k^f \triangleright Eq. (2.7).

3: Estimate the Kalman gain \mathbf{K}_k^l \triangleright Eq. (2.5b).

4: Evaluate the assimilated ensemble $\{\mathbf{q}_k^{a(1)}, \dots, \mathbf{q}_k^{a(N)}\}$ \triangleright Eq. (2.8).

5: **return** assimilated ensemble $\{\mathbf{q}_k^{a(1)}, \dots, \mathbf{q}_k^{a(N)}\}$.

Remark 1 (Enhance the linearity of the model M_k by reducing the observation time interval).

For nonlinear RODEs, an approach for increasing the validity of a linear approximation of the model M_k is reducing the observation time interval, $t_{k+1} - t_k$. When the observation map is linear and the RVs Q_0 and Ξ_k are assumed Gaussian, this approach is useful for extending the applicability of the (En)KF for nonlinear dynamical systems. However, reducing the observation time interval may not be practical because of its high operational costs or technical limitations, as mentioned earlier.

Remark 2 (Bias errors of the EnKF). Owing to the use of a linear filtering map, in the nonlinear setting, a bias error (i.e., a systematic error) exists when approximating the posterior density $\pi_{Q_k^f | Y_k^f}(\cdot | \hat{\mathbf{y}})$ using the assimilated ensemble given in Eq. (2.8). In particular, it is not guaranteed that the ensemble mean $\frac{1}{N} \sum_{i=1}^N \mathbf{q}_k^{a(i)}$ converges (in the sense of distribution) to $\int_{\mathbb{R}^n} \mathbf{q} \pi_{Q_k^f | Y_k^f}(\mathbf{q} | \hat{\mathbf{y}}) d\mathbf{q}$ as $N \rightarrow \infty$. Further discussion on the behavior of the EnKF with $N \rightarrow \infty$, which is also known as the mean-field filter, can be found in the literature [20]. In Secs. 3 and 4, we show that the EnCMF guarantees such a convergence.

3. Conditional mean filter. In this section, we present and analyze the conditional mean filter (CMF) and its ensemble version (EnCMF). First, we recall some useful basic properties of the conditional expectation tailored for the analysis step of the CMF in Sec. 3.1. Second, we discuss two particular cases, namely, the CM and the conditional variance, in more detail in Sec. 3.2. Using the CM, the assimilated ensemble mean of the EnCMF is identical to that of the posterior distribution. We also discuss the orthogonal projection property of the conditional expectation, which is not only a significant theoretical result but also allow for the ANN-based approximation of the CM presented in Sec. 4. Third, in Sec. 3.3, the CMF and its ensemble version are presented, and their properties are analyzed. Finally, in Sec. 3.4, we exemplify the EnCMF using a simple static inverse problem that highlights its differences from the EnKF.

3.1. Conditional expectation. Because our focus is on the *analysis* step of the filtering setting, we ignore subscript k from here onward whenever possible to simplify the notations. Let σ_{Y^f} be the σ -algebra generated by the observation RV Y^f and $r : \mathbb{R}^n \rightarrow \mathbb{R}$ be an arbitrary function such that $r \circ Q^f$ — a RV composed of the forecast state RV Q^f and the function r — has a finite expected absolute value (i.e., $r \circ Q^f \in L_1(\Omega, \mathbb{R}, \mathbb{P})$). The conditional expectation $\mathbb{E}[r \circ Q^f | Y^f]$ is a σ_{Y^f} -measurable RV defined as follows:

$$(3.1) \quad \int_A \mathbb{E}[r \circ Q^f | Y^f](\omega) \mathbb{P}(d\omega) = \int_A r \circ Q^f(\omega) \mathbb{P}(d\omega), \quad \forall A \in \sigma_{Y^f}.$$

The general theoretical properties of the conditional expectation can be found in the literature [6] and [10, Chapter 4]. Using Eq. (3.1) with $A = \Omega$, we immediately obtain

$$(3.2) \quad \mathbb{E}[\mathbb{E}[r \circ Q^f | Y^f]] = \mathbb{E}[r \circ Q^f],$$

which is known as the law of total expectation. According to the Doob-Dynkin lemma, $\mathbb{E}[r \circ Q^f | Y^f]$, as a σ_{Y^f} -measurable function, takes the form $\phi_{r \circ Q^f}(Y^f)$ for some almost surely unique measurable function $\phi_{r \circ Q^f}$ [6]. The following two key properties of the conditional expectation motivate us to use it in the proposed filtering framework, which will be discussed in Sec. 3.3.

First, the conditional expectation can be expressed using the conditional distribution, as suggested by its appellation. We obtain

$$(3.3) \quad \mathbb{E}[r \circ Q^f | Y^f](\omega) \equiv \phi_{r \circ Q^f}(Y^f(\omega)),$$

\mathbb{P} -almost surely, where $\phi_{r \circ Q^f}(\mathbf{y})$ is the mean of the conditioned RV $r(Q^f)|_{Y^f=\mathbf{y}}$. Assuming that the joint density π_{Q^f, Y^f} exists, then the function $\phi_{r \circ Q^f}$ in Eq. (3.3) is obtained as

$$(3.4) \quad \phi_{r \circ Q^f}(\mathbf{y}) = \int r(\mathbf{q}) \pi_{Q^f | Y^f}(\mathbf{q} | \mathbf{y}) d\mathbf{q},$$

where $\pi_{Q^f | Y^f}$ is the conditional density expressed in Eq. (2.3). Hence, the conditional expectation is a useful mean for characterizing the posterior distribution, particularly when combined with the following property.

Second, the conditional expectation has a geometric interpretation as the L_2 projection of the RV $r \circ Q^f$ onto the σ -algebra generated by the observation RV Y^f . In other words, assuming that the variances of the RVs Q^f , $r \circ Q^f$, and Y^f are finite, the map $\phi_{r \circ Q^f}$ satisfies

$$(3.5) \quad \phi_{r \circ Q^f} = \arg \min_{g \in \mathcal{S}(\mathbb{R}^m, \mathbb{R})} \mathbb{E} \left[|g \circ Y^f - r \circ Q^f|^2 \right],$$

where $\mathcal{S}(\mathbb{R}^m, \mathbb{R})$ is the set of all functions $g : \mathbb{R}^m \rightarrow \mathbb{R}$ such that the variance of the RV $g(Y^f)$ is finite. The orthogonal projection property is a crucial result that allows the approximation of the CM as a minimum MSE estimator of the RV Q^f in the σ -algebra σ_{Y^f} , which is presented in Sec. 3.2. For the reader's convenience, these two properties are discussed in more detail with proofs in Appendices A and B, respectively.

3.2. Conditional mean and variance. For developing our filter, we use two particular cases of the conditional expectation: the CM as the main ingredient of the filter and the conditional variance for analyzing the variance of the assimilated RVs.

Conditional mean. The CM $\mathbb{E} [Q^f | Y^f]$ is the vector-valued RV $\mathbb{E} [Q^f | Y^f] := \phi_{Q^f} \circ Y^f$ for some unique function $\phi_{Q^f} : \mathbb{R}^m \rightarrow \mathbb{R}^n$. Using the result presented in Eq. (3.4), the evaluation of the map ϕ_{Q^f} at \mathbf{y} is identical to the mean of the conditional density $\pi_{Q^f | Y^f}(\cdot | \mathbf{y})$:

$$(3.6) \quad \phi_{Q^f}(\mathbf{y}) = \int \mathbf{q} \pi_{Q^f, Y^f}(\mathbf{q} | \mathbf{y}) d\mathbf{q}.$$

Particularly, $\phi_{Q^f}(\hat{\mathbf{y}})$, which is obtained by evaluating the map ϕ_{Q^f} with the observation data $\hat{\mathbf{y}}$, is the mean of the Bayesian posterior density $\pi_{Q^f, Y^f}(\cdot | \hat{\mathbf{y}})$.

Remark 3 (CM in the linear-Gaussian setting). For the linear-Gaussian setting, $\pi_{Q^f, Y^f}(\cdot | \mathbf{y})$ is a Gaussian density with a mean value equal to $\mathbb{E} [Q^f] + \mathbf{K}^l(\mathbf{y} - \mathbb{E} [Y^f])$, which is obtained straightforwardly by taking the expectation of the assimilated RV in the KF in Eq. (2.5a) [17]. Thus, the map ϕ_{Q^f} is linear in that setting, i.e., $\phi_{Q^f}(\mathbf{y}) \equiv \mathbb{E} [Q^f] + \mathbf{K}^l(\mathbf{y} - \mathbb{E} [Y^f])$.

Using the orthogonal projection property (Eq. (3.5)), the CM can be identified as follows

$$(3.7) \quad \mathbb{E} [Q^f | Y^f] = \phi_{Q^f}(Y^f), \quad \text{where} \quad \phi_{Q^f} = \arg \min_{g \in \mathcal{S}(\mathbb{R}^m, \mathbb{R}^n)} \mathbb{E} \left[\|g \circ Y^f - Q^f\|^2 \right],$$

where $\mathcal{S}(\mathbb{R}^m, \mathbb{R}^n)$ is the set of all functions $g : \mathbb{R}^m \rightarrow \mathbb{R}^n$ such that the variance of the RV $g(Y^f)$ is finite, and $\| \cdot \|$ denotes the usual Euclidean norm. When limiting the function g in Eq. (3.7) to be linear, the sub-optimal approximation of the CM has a closed-form, which is given in the following lemma.

Lemma 3.1 (Linear approximation of the CM). The linear approximation g_l of the map ϕ_{Q^f} is defined as the orthogonal projection of RV Q^f onto the sub- σ -algebra $\sigma_{Y^f}^l = \{g_l^* \circ Y^f\}$ for all linear functions $g_l^* : \mathbb{R}^m \rightarrow \mathbb{R}^n$. The map g_l can be analytically obtained as follows:

$$(3.8) \quad g_l(\mathbf{y}) = \mathbf{K}\mathbf{y} + \mathbf{b},$$

where \mathbf{K} is the generalized Kalman gain,

$$(3.9) \quad \mathbf{K} = \mathbb{C}\text{ov} \left[Q^f, Y^f \right] \mathbb{C}\text{ov} \left[Y^f \right]^{-1},$$

and $\mathbf{b} = \mathbb{E} [Q^f - \mathbf{K}Y^f]$.

Appendix C presents a proof of this linear approximation. The generalized Kalman gain is identical to its original version \mathbf{K}^l (Eq. (2.5b)) for the linear-Gaussian setting.

Conditional variance. The conditional covariance matrix $\text{Cov} [Q^f | Y^f]$ is an $n \times n$ -matrix valued RV defined as follows

$$(3.10) \quad \text{Cov} [Q^f | Y^f] \equiv \mathbb{E} [Q^f Q^{f\top} | Y^f] - \mathbb{E} [Q^f | Y^f] \mathbb{E} [Q^f | Y^f]^\top.$$

3.3. Ensemble conditional mean filter. The mean of the posterior density $\pi_{Q^f | Y^f}(\cdot | \hat{\mathbf{y}})$ coincides with the CM evaluated at $\hat{\mathbf{y}}, \phi_{Q^f}(\hat{\mathbf{y}})$; hence, it is desirable to design a filter such that its assimilated RV also has the mean value $\phi_{Q^f}(\hat{\mathbf{y}})$. This filter should also agree with the KF in the case of the linear-Gaussian setting. The CMF proposed by Matthies et al. [27] fulfills these requirements. The CMF formulates the assimilated RV as follows

$$(3.11) \quad Q^a = Q^f + \phi_{Q^f}(\hat{\mathbf{y}}) - \phi_{Q^f}(Y^f).$$

The transformation in Eq. (3.11) is a nonlinear approximation of the general form \mathcal{T} in Eq. (2.4). Although the CMF was previously proposed [27], the literature focused only on the linear version, i.e., using Lemma 3.1 for approximating the CM. This linear version will be discussed in more detail in Remark 4. Here, we aim to develop a nonlinear approximation of the CMF. The useful theoretical properties of the CMF, particularly its relation to the (En)KF and the posterior distribution, are discussed in the following theorem.

Theorem 3.2 (Main properties of the CMF). *The assimilated RV obtained using the CMF in Eq. (3.11) satisfies the following properties:*

A) *For the linear-Gaussian setting, see explanation in Sec. 2, the CMF coincides with the KF, such that*

$$(3.12) \quad Q^f + \phi_{Q^f}(\hat{\mathbf{y}}) - \phi_{Q^f}(Y^f) \equiv Q^f + \mathbf{K}^l(\hat{\mathbf{y}} - Y^f).$$

B) *The mean of the RV Q^a expressed in Eq. (3.11) is identical to that of the Bayesian posterior density $\pi_{Q^f | Y^f}(\cdot | \hat{\mathbf{y}}_k)$ (Eq. (2.3)):*

$$(3.13) \quad \mathbb{E} [Q^a] = \phi_{Q^f}(\hat{\mathbf{y}}),$$

C) *The covariance of the RV Q^a expressed in Eq. (3.11) is equal to the expected conditional variance:*

$$(3.14) \quad \text{Cov} [Q^a] = \mathbb{E} [\text{Cov} [Q^f | Y^f]].$$

Proof. A) For the linear-Gaussian setting, we achieve that $\phi_{Q^f}(Y^f) \equiv \mathbf{K}^l Y^f + \mathbf{b}$ using Lemma 3.1. The assimilated RV obtained using the CMF Q^a becomes $Q^a = Q^f + \mathbf{K}^l(\hat{\mathbf{y}} - Y^f)$, which is identical to the KF (Eq. (2.5a)).

B) Let Q^I be defined as $Q^I := Q^f - \mathbb{E} [Q^f | Y^f]$. Based on the law of total expectation, we obtain the mean and variance of Q^I as follows:

$$(3.15) \quad \mathbb{E} [Q^I] = \mathbf{0}_n,$$

where $\mathbf{0}_n$ is the n -dimensional zeros vector, and

$$(3.16) \quad \text{Cov} [Q^I] = \text{Cov} [Q^f] - \text{Cov} \left[\mathbb{E} [Q^f | Y^f] \right],$$

respectively. Thus, the mean of the assimilated RV Q^a is identical to $\phi_{Q^f}(\hat{\mathbf{y}})$:

$$(3.17) \quad \mathbb{E} [Q^a] = \mathbb{E} [Q^I] + \phi_{Q^f}(\hat{\mathbf{y}}) = \phi_{Q^f}(\hat{\mathbf{y}}),$$

which is the mean of the Bayesian posterior density as expressed in Eq. (3.6).

C) Using the law of total variance

$$(3.18) \quad \text{Cov} [Q^f] = \mathbb{E} \left[\text{Cov} [Q^f | Y^f] \right] + \text{Cov} \left[\mathbb{E} [Q^f | Y^f] \right],$$

we obtain

$$(3.19) \quad \text{Cov} [Q^a] = \text{Cov} [Q^f] - \text{Cov} \left[\mathbb{E} [Q^f | Y^f] \right] = \mathbb{E} \left[\text{Cov} [Q^f | Y^f] \right]. \quad \blacksquare$$

Point A of Theorem 3.2 indicates that the CMF is a natural extension of the KF. Compared with the Bayesian posterior density, $\pi_{Q^f | Y^f}(\cdot | \hat{\mathbf{y}})$, the assimilated RV Q^a of the CMF expressed in Eq. (3.11) shows an identical mean vector, while its density generally does not match the posterior. In particular, the covariance matrix, $\text{Cov} [Q^a]$, of the assimilated RV of the CMF is not identical to that of the Bayesian posterior density $\text{Cov} [Q^f | Y^f = \hat{\mathbf{y}}]$, except for special cases such as the linear-Gaussian setting. However, as the expected conditional variance (Theorem 3.2, point C), the covariance matrix $\text{Cov} [Q^a]$ is an *optimal* prediction of the posterior covariance when the actual measurement data $\hat{\mathbf{y}}$ are not yet available. A fast approximation of the assimilated RV Q^a after acquiring the observation data $\hat{\mathbf{y}}$ is a practical requirement; thus, the filter components requiring intensive computational resources for approximation, e.g., the Kalman gain in the (En)KF or the CM in the CMF, should be approximated in advance. In this case, the *optimal* prediction of the posterior covariance obtained using the CMF is a significant advantage.

Ensemble conditional mean filter. Similar to the EnKF, the EnCMF uses the ensemble technique to represent the forecast and assimilated RVs. In the forecast step, the distributions of the RVs Q^f and Y^f are approximated using the ensembles of size N , $\{\mathbf{q}^{f(1)}, \dots, \mathbf{q}^{f(N)}\}$ and $\{\mathbf{y}^{f(1)}, \dots, \mathbf{y}^{f(N)}\}$, respectively, as expressed in Eq. (2.2). In the analysis step, the assimilated ensemble $\{\mathbf{q}^{a(1)}, \dots, \mathbf{q}^{a(N)}\}$ of the RV Q^a is evaluated using Eq. (3.11):

$$(3.20) \quad \mathbf{q}^{a(i)} = \mathbf{q}^{f(i)} + \phi_{Q^f}(\hat{\mathbf{y}}) - \phi_{Q^f}(\mathbf{q}^{f(i)}), \quad i = 1, \dots, N.$$

Implementing the EnCMF requires the evaluation of the map ϕ_{Q^f} of the CM. This task can be performed using two approaches: a) by evaluating of the conditional density in Eq. (3.6) and b) using the orthogonal projection property expressed in Eq. (3.7). The first approach has limited applicability for data assimilation problems with high-dimensional state-spaces because it requires approximating the density of the forecast RV Q^f for each assimilation step; moreover, the conditional distribution can be intractable. The latter approach is favorable in such a situation. In Sec. 3.4, we implement the EnCMF with a simple example, in which the first approach is applied. In Sec. 4, we discuss the approximation of the CM using the second approach.

Remark 4 (Optimal linear filter—a special case of the CMF). When approximating the CM using the optimal linear map provided in Lemma 3.1, we obtain the optimal linear filter and its ensemble version, which we refer herein as the generalized EnKF (gEnKF):

$$(3.21a) \quad Q^a = Q^f + \mathbf{K}(\hat{\mathbf{y}} - Y^f),$$

$$(3.21b) \quad \mathbf{q}^{a(i)} = \mathbf{q}^{f(i)} + \mathbf{K}(\hat{\mathbf{y}} - \mathbf{y}^{f(i)}), \quad i = 1, \dots, N,$$

where \mathbf{K} is the generalized Kalman gain expressed in Eq. (3.9), and the forecast ensembles are computed using Eqs. (2.6, 2.8). Compared with the usual EnKF, the only difference in the gEnKF is the use of the generalized Kalman gain (Eq. (3.9)), instead of its original one (Eq. (2.5b)). Consequently, the gEnKF is an extension of the EnKF for the nonlinear setting, particularly with nonlinear observation maps, for which the original Kalman gain is not applicable. As a linear approximation of the CMF (Eq. 3.11), the gEnKF no longer preserves the properties discussed in points B and C in Theorem 3.2. In Sec. 3.4, we present a comparison among the gEnKF, the EnCMF, and the Bayesian filter applied for a simple static inverse problem.

3.4. Illustration of the CMF for a simple static inverse problem. We consider the following inverse problem to compare the EnCMF with the EnKF and the ideal Bayesian filter. Given a one-dimensional RV $Q^f \sim \mathcal{N}(0, 2^2)$ and the following nonlinear observation map,

$$(3.22) \quad Y^f = h(Q^f) + \Xi \quad \text{where} \quad h(q) = \begin{cases} q & \text{if } q \leq 0 \\ q^2 & \text{if } q > 0 \end{cases}, \quad \Xi \sim \mathcal{N}(0, 0.5^2),$$

the task is to evaluate the Bayesian posterior for different values of the observation \hat{y} . We solve the problem using the EnCMF and gEnKF and compare their assimilated ensembles with the Bayesian posterior in terms of three statistical characteristics: mean, variance, and density. The observation map considered here is nonlinear; therefore, instead of using the original EnKF, we employ its generalized version, as explained in Remark 4.

For this simple problem, the map ϕ_{Q^f} of the CM is evaluated using Eq. (3.6) by employing the Monte Carlo (MC) method with 10000 samples. We refer to Eq. (3.9) and apply the MC method with the same number of samples as before to approximate the Kalman gain. For comparison, Fig. 3.1 depicts the CM map ϕ_{Q^f} with its linear approximation, which is obtained using Eq. (3.8). We observe an important error in the linear approximation. Consequently, a significant bias between the means of the assimilated ensemble of the gEnKF and the Bayesian posterior is predicted.

Using Theorem A.1, we approximate the conditional expectation of the second moment $\mathbb{E}[(Q^f)^2 | Y^f]$ and the conditional variance $\text{Var}[Q^f | Y^f]$ as follows

$$(3.23a) \quad \mathbb{E} \left[(Q^f)^2 | Y^f = y \right] = \int q^2 \pi_{Q^f | Y^f}(q | y) dq,$$

$$(3.23b) \quad \begin{aligned} \text{Var}[Q^f | Y^f] &= \mathbb{E} \left[(Q^f)^2 | Y^f \right] - \left(\mathbb{E} \left[Q^f | Y^f \right] \right)^2 \\ &= \mathbb{E} \left[(Q^f)^2 | Y^f \right] - \left(\phi_{Q^f}(Y^f) \right)^2, \end{aligned}$$

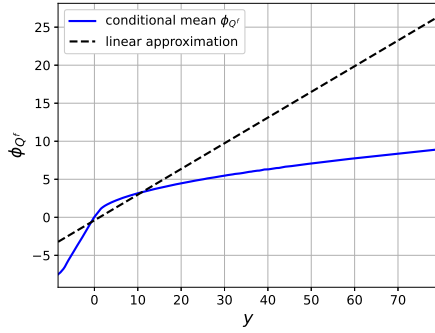


Figure 3.1: CM computed using Eq. (3.6) and its linear approximation (Eq. (3.8)).

where we employ the MC method to approximate the conditional expectation of the second moment in Eq. (3.23a). Fig. (3.2) presents the empirical cdf of the conditional variance. We

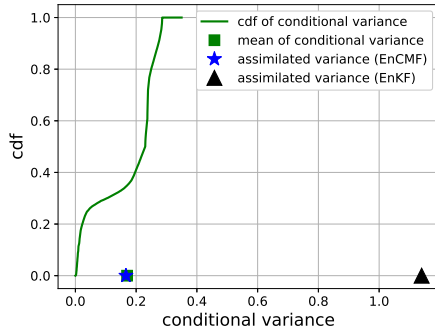


Figure 3.2: Empirical cdf of the conditional variance $\text{Var}[Q^f|Y^f]$ expressed in Eq. (3.23b) compared with the variances of the assimilated ensembles obtained using the EnKF and EnCMF. The expected conditional variance, $\mathbb{E}[\text{Var}[Q^f|Y^f]]$, and the assimilated ensemble variance of the EnCMF show closely identical estimated values of approximately 0.17.

implement the gEnKF, using Eqs. (2.6, 3.21b), and the EnCMF, using Eqs. (2.6, 3.20). We select a significantly large ensemble size of 10000 for both filters to ensure that the statistical errors are negligible. Fig. 3.2 depicts the theoretical statement in point C in Theorem 3.2. The assimilated ensemble variances in both filters are invariant with respect to varying of the measurement data. However, for the EnCMF, the assimilated ensemble variance is a non-biased estimator of the mean of the conditional variance; thus the EnCMF shows significant improvement in estimating the conditional variance than the gEnKF.

We consider different observation scenarios using various q^{true} values to evaluate the *synthesized* observation data as $\hat{y} = h(q^{\text{true}}) + \xi$ where ξ is an i.i.d. sample of the error RV Ξ . Fig. 3.3 presents the empirical densities of assimilated ensembles and the Bayesian poste-

rior density. Although the empirical density of the assimilated ensemble obtained using the EnCMF does not coincide with the Bayesian posterior, it still fits the posterior significantly better than that of the gEnKF. In particular, the assimilated ensemble mean obtained using the EnCMF is closely identical to the Bayesian posterior mean and in good agreement with the truth value q^{true} . In contrast, the assimilated ensemble of the EnKF exhibits significant biased errors in terms of the mean value compared with the Bayesian posterior. This numerical experiment reconfirms the theoretical statement in Theorem 3.2.

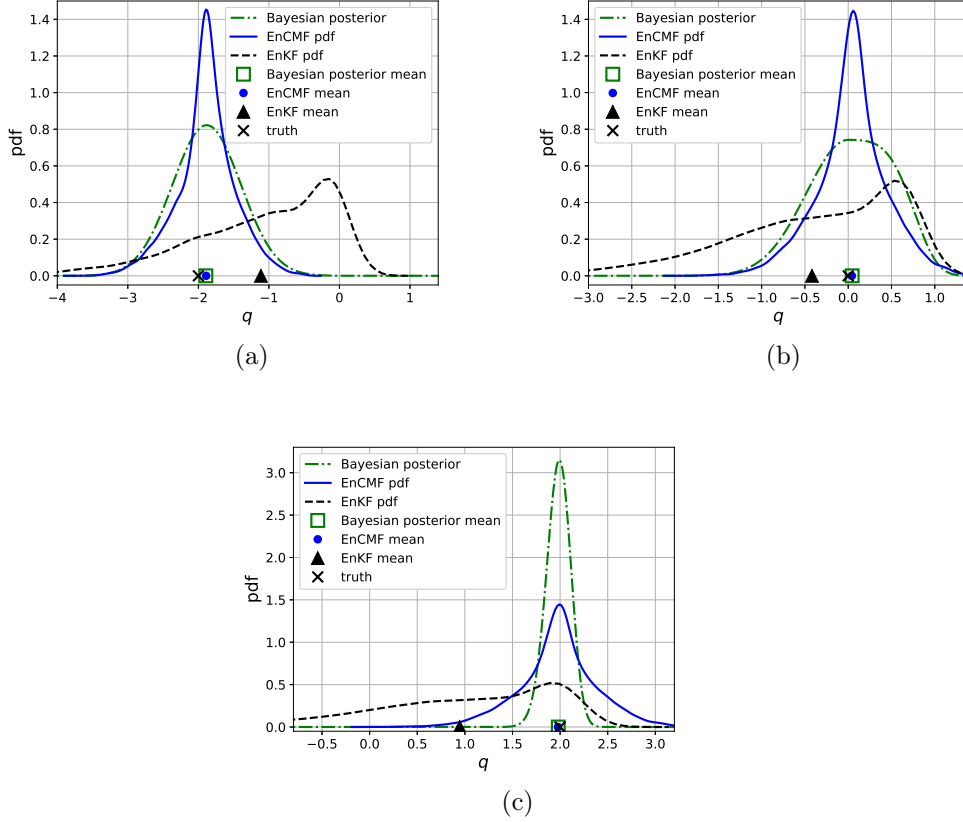


Figure 3.3: Comparison of the empirical densities of the assimilated ensembles and the Bayesian posterior: (a) actual value $q^{\text{true}} = -2$ (minus standard deviation of the prior distribution), (b) actual value $q^{\text{true}} = 0$ (mean of the prior distribution), (c) actual value $q^{\text{true}} = +2$ (plus standard deviation of the prior distribution).

4. ML-based EnCMF. In this section, we present the ML-EnCMF, which is a numerical implementation of the EnCMF using ML techniques. Based on the orthogonal projection property (Eq. (3.7)) we develop a CM approximation using ANNs trained using forecast ensembles. We obtain the assimilated ensemble by inserting the CM approximation in Eq. (3.20). Here, we describe the methodological aspect in more detail.

4.1. ANN approximation of the conditional mean. Let $g_{NN}(\cdot; \boldsymbol{\theta}) : \mathbb{R}^m \rightarrow \mathbb{R}^n$ be an ANN map, where $\boldsymbol{\theta}$ denotes its hyper-parameters, which are the network's weights and biases. The ANN structure is not fixed and adapted following the natural representation of the states. For example, convolution neural networks can be used for spatial/field states to represent the spatial correlation, while for the vector cases, feed-forward ANNs can be used, as described in Sec. 5. Here, we approximate the CM, that is the map ϕ_{Q^f} , by combining the linear approximation g_l (Eq. (3.8)), and the ANN $g_{NN}(\cdot; \boldsymbol{\theta})$ as

$$(4.1) \quad \phi_{Q^f}(\cdot) \approx g_l(\cdot) + a g_{NN}(\cdot; \boldsymbol{\theta}),$$

where $a \in \{0, 1\}$ is the activation parameter identified using the model selection procedure, which is explained in Sec. 4.2. After the ANN g_{NN} is trained, given the observation data $\hat{\mathbf{y}}$, the assimilated RV Q^a of the CMF (Eq. (3.11)) and its ensemble (Eq. (3.20)) are approximated by the following relations

$$(4.2a) \quad Q^a = Q^f + \mathbf{K}(\hat{\mathbf{y}} - Y^f) + a(g_{NN}(\hat{\mathbf{y}}; \boldsymbol{\theta}) - g_{NN}(Y^f; \boldsymbol{\theta})),$$

$$(4.2b) \quad \mathbf{q}^{a(i)} = \mathbf{q}^{f(i)} + \mathbf{K}(\hat{\mathbf{y}} - \mathbf{y}^{f(i)}) + a(g_{NN}(\hat{\mathbf{y}}; \boldsymbol{\theta}) - g_{NN}(\mathbf{y}^{f(i)}; \boldsymbol{\theta})), \quad i = 1, \dots, N,$$

respectively. Instead of relying solely on the ANN to approximate the map ϕ_{Q^f} , the combination in Eq. (4.1) is more robust. Only the nonlinearity of map ϕ_{Q^f} is approximated using an ANN; hence the proposed combination benefits from the approved performance of the EnKF in closely linear-Gaussian settings. Moreover, training ANNs on small datasets can lead to overfitting. Owing to the model selection procedure, the overfitting regime can be indicated and avoided by allowing the parameter a to be equal to zero, which will be discussed in Sec. 4.2.

We train the ANN g_{NN} by using the orthogonal projection property of the CM stated in Eq. (3.7). For a given tensor of hyper-parameters $\boldsymbol{\theta}$, we use the MSE $\mathcal{M}(\boldsymbol{\theta})$ defined as

$$(4.3) \quad \mathcal{M}(\boldsymbol{\theta}) = \mathbb{E} \left[\|Q^f - g_l(Y^f) - g_{NN}(Y^f; \boldsymbol{\theta})\|^2 \right]$$

as a metric for the approximation in Eq. (4.1). The hyper-parameters of the ANN are obtained by solving the following optimization problem

$$(4.4) \quad \boldsymbol{\theta} = \arg \min_{\boldsymbol{\theta}_*} \mathcal{M}(\boldsymbol{\theta}_*) + \mathcal{R}(\boldsymbol{\theta}_*),$$

where $\mathcal{R}(\boldsymbol{\theta}_*)$ is a regularization term applied to reduce overfitting, usually composed of L_1 or L_2 norms of the weights [9].

In our approach, the metric $\mathcal{M}(\boldsymbol{\theta})$ is estimated using the forecast ensembles. Let $\mathcal{D} = \{(\mathbf{y}^{f(1)}, \mathbf{q}^{f(1)}), \dots, (\mathbf{y}^{f(N)}, \mathbf{q}^{f(N)})\}$ be the dataset comprising of pairs $(\mathbf{y}^{f(i)}, \mathbf{q}^{f(i)})$ collected from the forecast ensembles. The dataset \mathcal{D} is divided into two sets: an N_T -sized training dataset \mathcal{D}_T for tuning the hyper-parameters and an N_S -sized test dataset \mathcal{D}_S for the testing the ANN; here, $N_T + N_S = N$. In both training and testing processes, the metric $\mathcal{M}(\boldsymbol{\theta})$ is estimated based on the corresponding datasets, \mathcal{D}_T and \mathcal{D}_S , respectively. Statistical errors are inherent in such an estimation; hence, we present a variance reduction technique to reduce these errors.

Reduced variance estimator of the MSE metric. The crude MC estimator of the metric \mathcal{M} using the training dataset is obtained as follows

$$(4.5) \quad \widehat{\mathcal{M}}(\boldsymbol{\theta}|\mathcal{D}_T) = \frac{1}{N_T} \sum_{(\mathbf{y}^{f(i)}, \mathbf{q}^{f(i)}) \in \mathcal{D}_T} \|\mathbf{q}^{f(i)} - g_l(\mathbf{y}^{f(i)}) - g_{NN}(\mathbf{y}^{f(i)}; \boldsymbol{\theta})\|^2.$$

We use the following reduced-variance estimator to reduce the statistical errors in evaluating the MSE metric

$$(4.6) \quad \widehat{\mathcal{M}}^{\text{vr}}(\boldsymbol{\theta}|\mathcal{D}_T) = \frac{1}{N_T} \sum_{(\mathbf{y}^{f(i)}, \mathbf{q}^{f(i)}) \in \mathcal{D}_T} \frac{1}{M} \sum_{j=1}^M \|\mathbf{q}^{f(i)} - g_l(h(\mathbf{q}^{f(i)}) + \boldsymbol{\xi}^{(i,j)}) - g_{NN}(h(\mathbf{q}^{f(i)}) + \boldsymbol{\xi}^{(i,j)}; \boldsymbol{\theta})\|^2,$$

which uses $N \times M$ sample $\boldsymbol{\xi}^{(i,j)}$ of the observation error Ξ instead of N used in the crude MC estimator. To motivate that $\widehat{\mathcal{M}}^{\text{vr}}$ may provide an estimation of \mathcal{M} with a reduced variance, we note that

$$(4.7) \quad \begin{aligned} \lim_{M \rightarrow \infty} \widehat{\mathcal{M}}^{\text{vr}}(\boldsymbol{\theta}|\mathcal{D}_T) &= \text{a.s.} \quad \frac{1}{N_T} \sum_{i=1, \dots, N_T} \mathbb{E}(\|\mathbf{q}^{f(i)} - g_l(h(\mathbf{q}^{f(i)}) + \Xi) - g_{NN}(h(\mathbf{q}^{f(i)}) + \Xi; \boldsymbol{\theta})\|^2) \\ &= \frac{1}{N_T} \sum_{i=1, \dots, N_T} \mathbb{E}[A(Q^f, \Xi; \boldsymbol{\theta}) | Q^f = \mathbf{q}^{f(i)}], \end{aligned}$$

\mathbb{P} -almost surely, where

$$(4.8) \quad A(\mathbf{q}, \boldsymbol{\xi}; \boldsymbol{\theta}) \equiv \|\mathbf{q} - g_l(h(\mathbf{q}) + \boldsymbol{\xi}) - g_{NN}(h(\mathbf{q}) + \boldsymbol{\xi}; \boldsymbol{\theta})\|^2.$$

Let $\widehat{\mathcal{M}}^{\text{vr}*}(\boldsymbol{\theta}|\mathcal{D}_T)$ denote the right-hand-side term in Eq. (4.7). To gain some further insight, let us assume that the ensemble members $q^{f(i)}$, $i = 1, \dots, N$, are i.i.d. samples for the sake of simplicity. We can then approximately quantify the statistical errors of the approximation $\widehat{\mathcal{M}}(\boldsymbol{\theta}|\mathcal{D}_T)$ and $\widehat{\mathcal{M}}^{\text{vr}}(\boldsymbol{\theta}|\mathcal{D}_T)$, respectively as

$$(4.9a) \quad \text{Var} \left[\widehat{\mathcal{M}}(\boldsymbol{\theta}|\mathcal{D}_T) - \mathcal{M}(\boldsymbol{\theta}) \right] = \frac{\text{Var}[A(Q^f, \Xi; \boldsymbol{\theta})]}{N_T},$$

$$(4.9b) \quad \text{Var} \left[\widehat{\mathcal{M}}^{\text{vr}*}(\boldsymbol{\theta}|\mathcal{D}_T^a) - \mathcal{M}(\boldsymbol{\theta}) \right] = \frac{\text{Var}[\mathbb{E}[A(Q^f, \Xi; \boldsymbol{\theta}) | Q^f]]}{N_T}.$$

Using the law of total variance,

$$(4.10) \quad \text{Var}[A(Q^f, \Xi; \boldsymbol{\theta})] = \text{Var}[\mathbb{E}[A(Q^f, \Xi; \boldsymbol{\theta}) | Q^f]] + \mathbb{E}[\text{Var}[A(Q^f, \Xi; \boldsymbol{\theta}) | Q^f]],$$

we obtain

$$(4.11) \quad \text{Var}[\mathbb{E}[A(Q^f, \Xi; \boldsymbol{\theta}) | Q^f]] \leq \text{Var}[A(Q^f, \Xi; \boldsymbol{\theta})].$$

Therefore, when M is sufficiently large, the estimator $\widehat{\mathcal{M}}^{\text{vr}}(\boldsymbol{\theta}|\mathcal{D}_T)$ shows minor statistical errors compared with $\widehat{\mathcal{M}}(\boldsymbol{\theta}|\mathcal{D}_T)$.

Intuitively, this variance reduction technique decreases the sensitivity of the trained ANN to observation noise because additional noisy data are used for training. From the implementation perspective, using the reduced-variance estimator $\widehat{\mathcal{M}}^{\text{vr}}(\boldsymbol{\theta}|\mathcal{D}_T)$ is equivalent to training the ANN on an augmented dataset:

$$(4.12) \quad \mathcal{D}^a = \{(\mathbf{y}^{f(i,j)}, \mathbf{q}^{f(i)}), \quad i = 1, \dots, N, \quad j = 1, \dots, M\} \quad \text{where } \mathbf{y}^{f(i,j)} = h(\mathbf{q}^{f(i)}) + \boldsymbol{\xi}^{(i,j)},$$

which does not require any modification of the implemented training algorithm.

4.2. Model selection. Training the ANN with possibly many hyper-parameters on small datasets can lead to overfitting. To alleviate this risk, we only use the high-dimensional and complex ANN model if it shows a significant improvement for the goodness-of-fit. Although the CM may be nonlinear, the linear approximation (Eq. (3.8)) may still be preferable over an ANN-based approximation that is significantly overfitted owing to robustness. We perform this model selection step based on the testing dataset $\mathcal{D}_S \subset \mathcal{D}$ and compare the MSE metrics between the trained ANN-based approximation and the linear counterpart to identify the value of parameter a in Eq. (4.1). We set parameter a to zero when the ANN-based approximation is underperforming compared with the linear one; otherwise, its value is set to one. Let \mathcal{M}_l be the MSE metric of the CM linear approximation, which is evaluated as $\mathcal{M}_l = \mathbb{E} [\|Q^f - g_l(Y^f)\|^2]$. We estimate parameter a using the following logic operator:

$$(4.13) \quad a = \mathbf{1}(\widehat{\mathcal{M}}_l^{\text{vr}} > \widehat{\mathcal{M}}^{\text{vr}}(\boldsymbol{\theta}|\mathcal{D}_S)),$$

where $\mathbf{1}(\cdot)$ is a logical operator yielding one if the condition (\cdot) is correct and zero otherwise. We use the variance reduction technique, similar to Eq. (4.6), for estimators $\widehat{\mathcal{M}}_l^{\text{vr}}$ and $\widehat{\mathcal{M}}^{\text{vr}}(\boldsymbol{\theta}|\mathcal{D}_S)$:

$$(4.14a) \quad \widehat{\mathcal{M}}_l^{\text{vr}} = \frac{1}{N_S} \sum_{(\mathbf{y}^{f(i)}, \mathbf{q}^{f(i)}) \in \mathcal{D}_S} \frac{1}{M} \sum_{j=1}^M \|\mathbf{q}^{f(i)} - g_l(h(\mathbf{q}^{f(i)}) + \boldsymbol{\xi}^{(i,j)})\|^2,$$

$$(4.14b) \quad \widehat{\mathcal{M}}^{\text{vr}}(\boldsymbol{\theta}|\mathcal{D}_S) = \frac{1}{N_S} \sum_{(\mathbf{y}^{f(i)}, \mathbf{q}^{f(i)}) \in \mathcal{D}_S} \frac{1}{M} \sum_{j=1}^M \|\mathbf{q}^{f(i)} - g_l(h(\mathbf{q}^{f(i)}) + \boldsymbol{\xi}^{(i,j)}) - g_{NN}(h(\mathbf{q}^{f(i)}) + \boldsymbol{\xi}^{(i,j)}; \boldsymbol{\theta})\|^2.$$

To avoid bias errors, the metrics $\widehat{\mathcal{M}}_l^{\text{vr}}$ and $\widehat{\mathcal{M}}^{\text{vr}}$ are estimated using the test dataset, which does not contain the training data.

4.3. Algorithms. Algorithms 4.1 and 4.2 summarize our ML-EnCMF implementation. The former presents a pseudo-code of the ML-EnCMF. The latter describes the ANN training and model selection procedures. In Algorithm 4.1, the forecast step and Kalman gain estimation are similar to those of the gEnKF; refer to Algorithm 2.1 and Remark 4. Given the forecast ensembles $\{\mathbf{q}_k^{f(1)}, \dots, \mathbf{q}_k^{f(N)}\}$, $\{\mathbf{y}_k^{f(1)}, \dots, \mathbf{y}_k^{f(N)}\}$ and estimated Kalman gain, we

approximate the map $\phi_{Q_k^f}$ using ANNs, for which the training pseudo-code is presented in Algorithm 4.2.

Algorithm 4.1 ML-EnCMF algorithm for performing assimilation at time t_k .

Require: Assimilated ensembles obtained from the assimilation step performed at t_{k-1} $\{\mathbf{q}_{k-1}^{a(1)}, \dots, \mathbf{q}_{k-1}^{a(N)}\}$ and observational data $\widehat{\mathbf{y}}_k$.

Forecast:

1: Evaluate forecast ensembles $\{\mathbf{q}_k^{f(1)}, \dots, \mathbf{q}_k^{f(N)}\}$ and $\{\mathbf{y}_k^{f(1)}, \dots, \mathbf{y}_k^{f(N)}\}$. \triangleright Eq. (2.6).

Analysis:

2: **if** observation map is linear **then**

3: Estimate the Kalman gain \mathbf{K}_k^l \triangleright Eq. (2.5b)

4: **else**

5: Estimate the generalized Kalman gain \mathbf{K}_k \triangleright Eq. (3.9)

6: Approximate the map $\phi_{Q_k^f}$ using ANN g_{NN} , see Eq. (4.1), by executing Algorithm 4.2.

7: Evaluate the assimilated ensemble $\{\mathbf{q}_k^{a(1)}, \dots, \mathbf{q}_k^{a(N)}\}$. \triangleright Eq. (4.2b).

8: **return** assimilated ensemble $\{\mathbf{q}_k^{a(1)}, \dots, \mathbf{q}_k^{a(N)}\}$.

Algorithm 4.2 Training algorithm of the ANNs used for approximation of the map ϕ_{Q^f} .

Require: Ensembles $\{\mathbf{q}^{f(1)}, \dots, \mathbf{q}^{f(N)}\}$ and $\{\mathbf{y}^{f(1)}, \dots, \mathbf{y}^{f(N)}\}$, number of epochs n_e , ANN g_{NN} , Kalman gain \mathbf{K} .

Initialization:

1: Set the initial hyper-parameters $\boldsymbol{\theta}^0$.

2: Generate $N \times M$ -size augmented dataset. \triangleright Eq. (4.12)

3: Compute the initial metric $m_0 = \widehat{\mathcal{M}}^{\text{vr}}(\boldsymbol{\theta}^0 | \mathcal{D}_S)$. \triangleright Eq. (4.14b).

Training:

4: **for** $\nu = 1, \dots, n_e$ **do**

5: Train ANN using mini-batch stochastic gradient descent method [18, 3] to update $\boldsymbol{\theta}^\nu$.

6: Compute the testing metric: $m_\nu = \widehat{\mathcal{M}}^{\text{vr}}(\boldsymbol{\theta}^\nu | \mathcal{D}_S)$ \triangleright Eq. (4.14b).

7: **If** $m_\nu < \min\{m_0, \dots, m_{\nu-1}\}$ **then**

8: $\boldsymbol{\theta} = \boldsymbol{\theta}^\nu$ \triangleright Call-back procedure

9: **end for**

Model selection:

10: Evaluate $\widehat{\mathcal{M}}_l^{\text{vr}}$. \triangleright Eq. (4.14a)

11: **if** $\min\{m_0, \dots, m_\nu\} < \widehat{\mathcal{M}}_l^{\text{vr}}$ **then**

12: $a = 1$

13: **else**

14: $a = 0$

15: **end if**

16: **return** hyper-parameters $\boldsymbol{\theta}$ and parameter a .

In Algorithm 4.2, using the forecast ensemble, $\mathcal{D} = \{(\mathbf{y}_k^{f(1)}, \mathbf{q}_k^{f(1)}), \dots, (\mathbf{y}_k^{f(N)}, \mathbf{q}_k^{f(N)})\}$,

we first generate the augmented dataset (Eq. (4.12)), which is used to compute the reduced-variance estimators of the MSE metric as expressed in Eqs. (4.6, 4.14b). Then, to solve the MSE minimizing problem described in Eq. (4.4), this algorithm uses the mini-batch version of the stochastic gradient descent method, which is a widely used approach for ANN training [18]. We include a call-back procedure into the training process to select the hyper-parameters with the best performance [14]. Finally, the model selection procedure (explained in Sec. 4.2) is performed.

5. Numerical experiments for Lorenz systems. In this section, we demonstrate the performance of ML-EnCMF for the data assimilation of Lorenz 63 (L63) and Lorenz 96 (L96) systems in comparison with the EnKF. Numerical studies on the influence of the ensemble size and variance reduction technique on the ML-EnCMF performance are also reported. Furthermore, we compare our proposed filtering method with those reported in the literature [22, 30].

5.1. Setup. In this subsection, we describe the setup of the considered data assimilation problems, particularly dynamical models, observation scenarios, and performance metrics.

5.1.1. Dynamical models.

Lorenz-63 system. The L63 model is a simplified model of atmospheric convection [23] comprising three ODEs:

$$(5.1) \quad \frac{dq_1}{dt} = \sigma(q_2 - q_1), \quad \frac{dq_2}{dt} = q_1(\rho - q_3) - q_2, \quad \frac{dq_3}{dt} = q_1q_2 - \beta q_3,$$

where q_1 , q_2 , and q_3 are proportional to the rate of convection, horizontal temperature variation, and vertical temperature variation, respectively, and σ , β , and ρ are the system parameters. We use $\sigma = 10$, $\beta = 8/3$, and $\rho = 28$ as a conventional setting of the L63 system, resulting in a chaotic behavior.

Lorenz-96 system. The L96 model is an idealized model of a one-dimensional latitude band of the Earth's atmosphere [24]. The system is defined using a set of ODEs over the periodic domain of a 40th-dimensional state vector, $\mathbf{q} = [q_1, q_2, \dots, q_n]$ with $n = 40$:

$$(5.2) \quad \frac{dq_i}{dt} = (q_{i+1} - q_{i-2})q_{i-1} - q_i + F, \quad i = 1, \dots, 40; \quad q_{n+1} = q_1,$$

where $q_0 = q_n$, $q_{-1} = q_{n-1}$, and F is the forcing constant. We select $F = 8$, which is known to cause a chaotic behavior.

For both models, the *synthesized* truth state vector at $t = 0$, $\mathbf{q}^{\text{true}}(t = 0)$, is given as a sample of the normal distribution $\mathcal{N}(\mathbf{0}_n, \mathbf{I}_n)$. The RV Q_0 is also assumed to follow this distribution. We simulate the L63 and L96 models using a fourth-order explicit Runge-Kutta algorithm with a time step $\Delta t = 0.01$.

5.1.2. Observation scenarios. For the L63 system, we assume that every state is observed using the following observation model:

$$(5.3) \quad \mathbf{y}_k = \mathbf{q}(t_k) + \boldsymbol{\xi}_k, \quad \boldsymbol{\xi}_k \sim \mathcal{N}(\mathbf{0}_3, 2^2 \mathbf{I}_3),$$

For the L96 system, the even-indexed states are observed using a linear map as follows

$$(5.4) \quad \mathbf{y}_k = \mathbf{H}\mathbf{q}(t_k) + \boldsymbol{\xi}_k, \quad \boldsymbol{\xi}_k \sim \mathcal{N}(\mathbf{0}_{20}, 0.5\mathbf{I}_{20}),$$

where $\mathbf{H} \in \mathbb{R}^{m \times n}$ with $m = 20$ is a linear operator that selects the even-indexed components $q_{k,2}, q_{k,4}, \dots, q_{k,40}$ from \mathbf{q}_k . We assume that the time interval ΔT_{obs} is constant, i.e., $\Delta T_{\text{obs}} = t_{k+1} - t_k$, for $k = 1, \dots, K-1$. In all the scenarios, we examine different observation time intervals ΔT_{obs} in the range [0.1, 2.]. For reference, $\Delta T_{\text{obs}} = 0.05$ is comparable to 6 h in a weather forecast model [25, 26].

5.1.3. Performance metrics. At each assimilation step k , the mean vector $\bar{\mathbf{q}}_k^a$ of the assimilated ensemble $\{\mathbf{q}_k^{a(1)}, \dots, \mathbf{q}_k^{a(N)}\}$ is compared with the truth state $\mathbf{q}^{\text{true}}(t_k)$ using the component-average root MSE (RMSE) criterion, $rmse_k$, which is defined as

$$(5.5) \quad rmse_k = \frac{\|\bar{\mathbf{q}}_k^a - \mathbf{q}^{\text{true}}(t_k)\|}{\sqrt{n}}, \quad k = 1, \dots, K.$$

We use the *median* and *average* of these values $\{rmse_1, \dots, rmse_K\}$ as performance metrics. We also monitor the average ensemble spread, \overline{ens} , defined as

$$(5.6) \quad \overline{ens} = \frac{1}{K} \sum_{k=1}^K \left[\frac{\text{tr}(\mathbb{Cov}[Q_k^a])}{n} \right]^{1/2},$$

to measure the contraction of the ensemble. In Eq. (5.6), $\text{tr}(\mathbb{Cov}[Q_k^a])$ is estimated from the ensemble $\{\mathbf{q}_k^{a(1)}, \dots, \mathbf{q}_k^{a(N)}\}$. The final metric that we consider herein is the average coverage probability f_{cv} of the 95%-confidence interval bounded between 2.5% and 97.5% quantiles of each marginal distribution, which is estimated as follows

$$(5.7) \quad f_{\text{cv}} = \frac{1}{n \times K} \sum_{k=1, \dots, K, i=1, \dots, n} \mathbf{1}(q_i^{\text{true}}(t_k) \in I_{i,k}),$$

where $I_{i,k}$ is the 95%-confidence interval of the i -th component of the assimilated ensemble at t_k . The aforementioned performance metrics are commonly used to evaluate data assimilation algorithms [22, 30, 21].

5.2. Lorenz 63 system. In this subsection, we report the numerical result of the proposed ML-EnCMF in tracking the L63 system. In our numerical example, we employ dense feed-forward ANNs to approximate the CM proposed in Eq. (4.1). We implement the ML-EnCMF with two different ANN structures to investigate the influence of the ANN structure on the performance of the ML-EnCMF: a) one-hidden layer ANN of the structure [3, 20, 3] and b) two-hidden layers ANN of the structure [3, 20, 20, 3]¹. The first structure is known as the shallow ANN, while the second structure is a deep version. The total numbers of hyper-parameters being trained are 142 and 563 for the first and second structures, respectively. We perform the

¹The first and last components are the numbers of the neurons of the input and output layers, respectively, the middle components are numbers of the neurons of the hidden layers.

ML-EnCMF with a large ensemble size, $N = 1000$, to isolate the effect of the ANN structure on the ML-EnCMF performance from other aspects. We also apply the variance reduction technique with $M = 10$. The forecast ensembles are divided into training and testing datasets with the size ratio of $N_T : N_S = 7 : 3$. At each assimilation step, we train the ANN for a maximum of 300 epochs and a learning rate of 0.001 using Algorithm 4.2.

Fig. 5.1 presents the obtained average RMSEs of the ML-EnCMFs implemented with different ANN structures compared with the EnKF for various observation time intervals $\Delta T_{\text{obs}} \in [0.1, 2]$. The results obtained using different ANN structures are closely identical, and only a slight improvement achieved by using the deep ANN version for $\Delta T_{\text{obs}} \in [0.4, 2]$. Hence, further increasing the ANN structure complexity is unnecessary. As shown in Fig. 5.1,

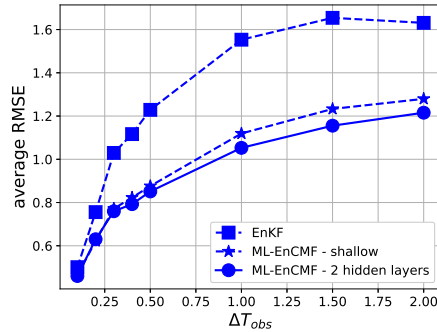


Figure 5.1: L63 system: comparison between the EnKF and ML-EnCMF in terms of the average RMSE for tracking the L63 system. In both filters, the ensemble size is fixed $N = 1000$. For ML-EnCMF, we select $M = 10$.

the ML-EnCMF's improvement compared with the EnKF is insignificant for short observation time intervals (e.g., $\Delta T_{\text{obs}} = 0.1$) but is becoming increasingly important for longer time intervals. For example, for $\Delta T_{\text{obs}} \in [0.3, 2]$, the relative improvements in terms of the average RMSE are observed in the range 23%-32%. For a short observation time interval (e.g., $\Delta T_{\text{obs}} = 0.1$), the assimilation problem is approximately linear-Gaussian, and the EnKF already provides a good approximation, as discussed in Remark 1. Thus, the performances of the EnKF and ML-EnCMF are similar for $\Delta T_{\text{obs}} = 0.1$. For a long observation time interval, the forecast RVs become strongly non-Gaussian; consequently, the ML-EnCMF outperforms the EnKF.

We implement the ML-EnCMF using the second ANN structure with different ensemble sizes ($N \in [60, 1000]$) to investigate the influence of the ensemble size and variance reduction technique proposed in Sec. 4 on the performance of the ML-EnCMF. Because significant small ensemble sizes are used, we select $M = 30$, which is larger than the previous study where $M = 10$ and the ensemble size is fixed at $N = 1000$. Fig. 5.2 presents a comparison between EnKF and ML-EnCMF in terms of the average RMSE, 95%-coverage probability, and average ensemble spread. We observe that the variance reduction technique is beneficial for significantly reduce the ensemble size. Without using the variance reduction technique, the convergence

in terms of performance is not observed for $N \leq 1000$. Alternatively, owing to the variance reduction technique, the EnCMF reaches its asymptotic performance from $N \approx 200$.

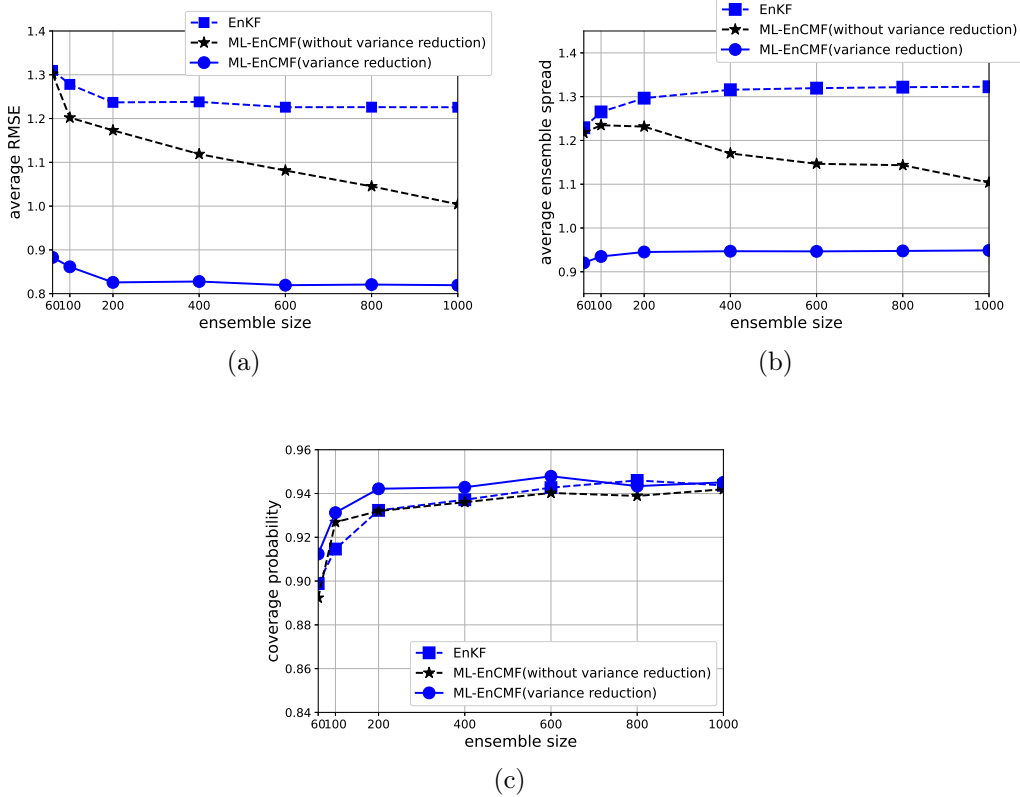


Figure 5.2: L63 system: influence of the ensemble size and variance reduction technique on the performances of the EnKF and ML-EnCMF for tracking the L63 system with $\Delta T_{\text{obs}} = 0.5$. (a) Average RMSE, (b) average ensemble spread, and (c) 95%-coverage probability.

Fig. 5.3 depicts the influence of the additional sample number M on the performance of the ML-EnCMF for the case $N=200$. Fig. 5.3 reconfirms the significant role of the variance reduction technique when the sample size is small. The M value at which no significant performance improvement is observed is 30 for $N = 200$.

5.3. Lorenz 96 system. Herein, we present the numerical result of the proposed filtering technique in tracking the L96 system under the partial observation scenario discussed in Sec. 5.1.2. We investigate the effect of the ANN structure on the performance of the ML-EnCMF by implementing the filter with two ANN structures: a) one-hidden-layer ANN [20, 30, 40] and b) two-hidden-layer ANN [20, 30, 30, 40]. The total numbers of hyper-parameters being trained are 3700 and 7360 for the first and second structures, respectively. Unlike the data assimilation problem in Sec. 5.2, where every element of the state vector is observed, in this example, only half is observable. For significantly large observation time intervals,

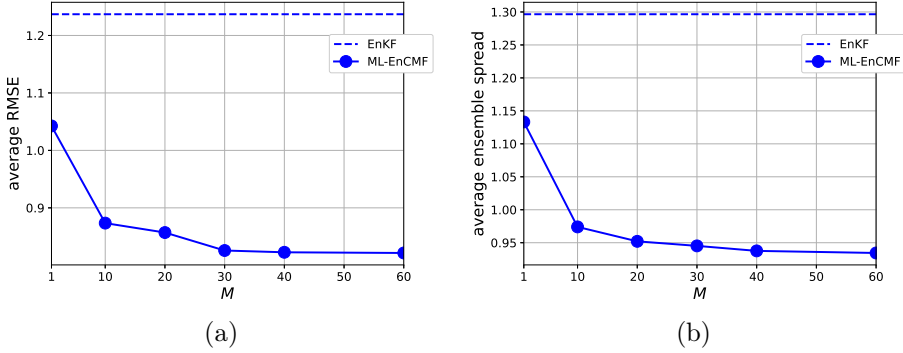


Figure 5.3: L63 system: influence of the additional sample number M on the performance of the ML-EnCMF for tracking the L63 system with $\Delta T_{\text{obs}} = 0.5$. (a) Average RMSE and (b) average ensemble spread.

inferring unobservable states using the measurement data of the observable ones becomes ineffective because their statistical dependence is reducing. We implement the filtering problem in this example with $\Delta T_{\text{obs}} \in [0.1, 0.5]$, which is a reduced range compared with that in Sec. 5.2, where $\Delta T_{\text{obs}} \in [0.1, 2]$. Taking advantage of the analysis in Sec. 5.2, we select $N = 1000$ and $M = 30$ and retain the other parameters similar to those in Sec. 5.2.

Fig. 5.4 shows the obtained average RMSEs of the ML-EnCMF implemented with different ANN structures and the EnKF. In agreement with the observation obtained in Sec. 5.2, using the deep ANN does not significantly improve the ML-EnCMF performance compared with the shallow structure. Moreover, the ML-EnCMF outperforms the EnKF for large observation time intervals ($\Delta T_{\text{obs}} \geq 0.4$), while their performances are comparable for small observation time intervals ($\Delta T_{\text{obs}} \leq 0.2$). Compared with the EnKF, the average RMSE of the ML-EnCMF is smaller by 22% and 25% for $\Delta T_{\text{obs}} = 0.4$ and $\Delta T_{\text{obs}} = 0.5$, respectively.

We implement the ML-EnCMF using the shallow ANN structure with different ensemble sizes ($N \in [60, 1000]$) to investigate the influence of the ensemble size on the performance of the ML-EnCMF. Fig. 5.5 presents the performances metric of the ML-EnCMF compared with the EnKF for different ensemble sizes. For $N \geq 600$, the ML-EnCMF decreases the average RMSE and the average ensemble spread by up to 22% and 20%, respectively. In terms of the coverage probability, the ML-EnCMF consistently outperforms the EnKF.

Finally, we compare the proposed method with two nonlinear ensemble filtering techniques reported in the literature: the moment-matching-based filter [22] and transport map-based filter [30]. The former matches the mean and variance of the assimilated ensembles with those of the posterior, which are estimated based on the likelihood function. The latter seeks a map for transforming the forecast RV to the assimilated RV that minimizes the Kullback-Leibler divergence to the posterior distribution. Table 5.1 reports a comparison in terms of the average and median RMSEs for the L96 system. The proposed method achieves a similar performance as the transport map-based filter and a significant improvement compared with

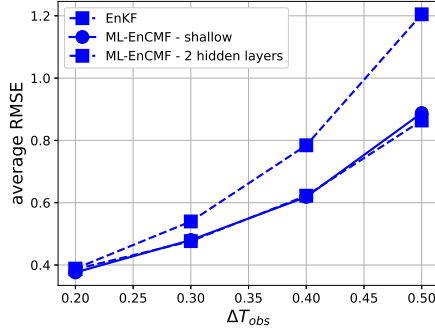


Figure 5.4: L96 system: comparison between the EnKF and ML-EnCMF in terms of the average RMSE. The ensemble size is fixed at $N = 1000$. For ML-EnCMF, we select $M = 30$.

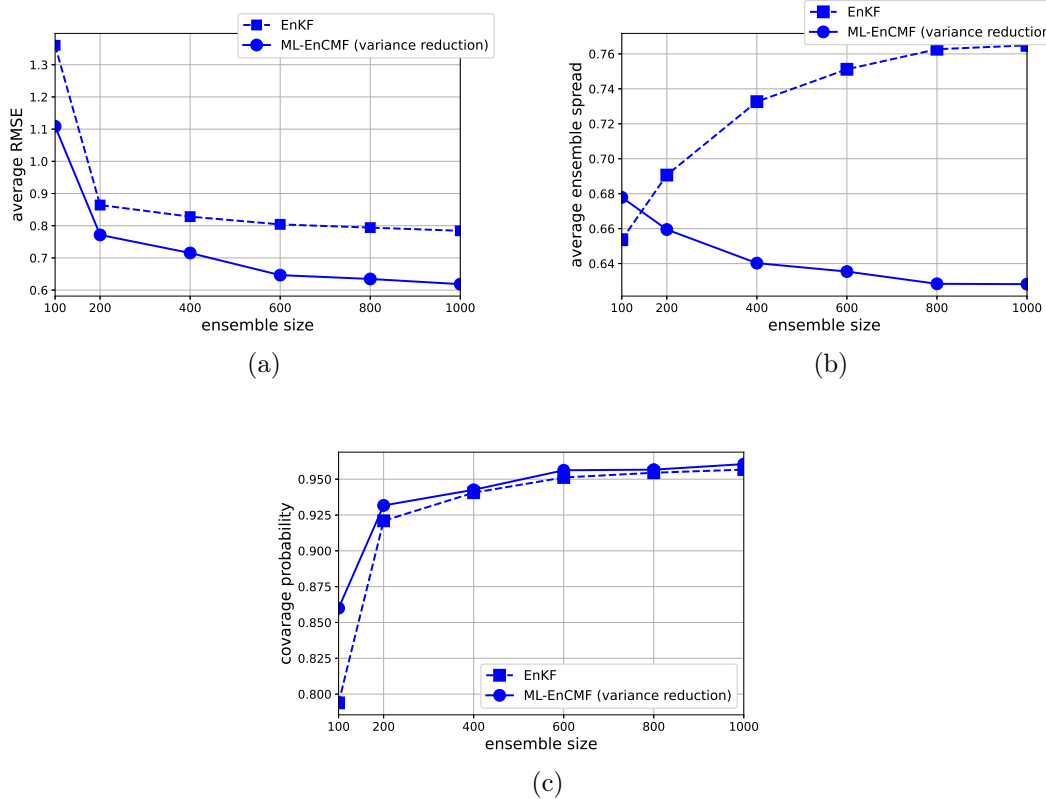


Figure 5.5: L96 system: influence of the ensemble size N on the performance of EnKF and ML-EnCMF for tracking L96 system with $\Delta T_{obs} = 0.4$. (a) average RMSE, (b) average ensemble spread, and (c) 95%-coverage probability.

the moment-matching filtering method.

Table 5.1: L96 system: performance metrics (average and median RMSE) of the ML-EnCMF compared with the moment-matching-based filter and transport map-based filter with $T=0.4$.

	Moment matching $N = 600$, Tab. 3 in [22]	Transport map $N = 600$, Fig. 9 in [30]	ML-EnCMF	
			$N = 600$	$N = 1000$
Average RMSE	0.68	0.61	0.64	0.62
Median RMSE	0.63	0.61	0.61	0.58

6. Conclusion. In this work, we develop the ML-EnCMF based on CM and show that the filter provides assimilated ensembles with a non-biased ensemble mean and optimal variance. Taking advantage of the conditional expectation as the best approximation with respect to the MSE, we employ ANNs to approximate the CM by minimizing the MSE metric, which is a critical part of the ML-EnCMF. This ML-based approach gains the filter flexibility for high-dimensional state-space data assimilation problems with nonlinear dynamics. The EnCMF performance is demonstrated for state-of-the-art data assimilation problems. In summary, the proposed filtering method exhibits considerable improvement compared with the commonly used methods, such as the EnKF. The EnCMF shows significant potential for filtering problems with spatiotemporally sparse observations.

Acknowledgment. This publication was supported by funding from the Alexander von Humboldt Foundation and King Abdullah University of Science and Technology (KAUST) Office of Sponsored Research (OSR) under award numbers URF/1/2281-01-01 and URF/1/2584-01-01 in the KAUST Competitive Research Grants Programs, respectively. R. Tempone is a member of the KAUST SRI Center for Uncertainty Quantification in Computational Science and Engineering. Simulations were performed with computing resources granted by RWTH Aachen University under project rwth0632.

Appendix A. Conditional expectation as a mean for characterizing conditional distribution.

Theorem A.1. *Assuming that the joint density π_{Q^f, Y^f} of RVs Q^f and Y^f exists, let $\phi_{r \circ Q^f}(\mathbf{y})$ be the conditioned mean of the RV $r(Q^f)$ given observation \mathbf{y} :*

$$(A.1) \quad \phi_{r \circ Q^f}(\mathbf{y}) = \int_{\mathbb{R}^n} r(\mathbf{q}) \pi_{Q^f | Y^f}(\mathbf{q} | \mathbf{y}) d\mathbf{q},$$

where $\pi_{Q^f | Y^f}(\cdot | \mathbf{y})$ is the conditional density expressed in Eq. (2.3). Then, the RV $\phi_{r \circ Q^f}(Y^f)$ is identical to the conditional expectation $\mathbb{E}[r \circ Q^f | Y^f]$, that is, satisfying the condition stated in Eq. (3.1).

Proof. The RV $\phi_{r \circ Q^f}(Y^f)$ is σ_{Y^f} -measurable following Doob-Dynkin lemma. To prove the Theorem A.1, we must verify the condition in Eq. (3.1). For any $A \in \sigma_{Y^f}$, let B be a

measurable set in \mathbb{R}^m such that $A = Y^f - 1(B) \equiv \{\omega : Y^f(\omega) \in B\}$, we obtain

$$\begin{aligned}
\int_A \phi_{r \circ Q^f}(Y^f) \mathbb{P}(\mathrm{d}\omega) &= \mathbb{E} \left[\phi_{r \circ Q^f}(Y^f) \mathbf{1}_B(Y^f) \right] \\
&= \int_B \phi_{r \circ Q^f}(\mathbf{y}) \pi_{Y^f}(\mathbf{y}) \mathrm{d}\mathbf{y} \\
&= \int_B \int_{\mathbb{R}^n} r(\mathbf{q}) \pi_{Q^f|Y^f}(\mathbf{q}|\mathbf{y}) \pi_{Y^f}(\mathbf{y}) \mathrm{d}\mathbf{q} \mathrm{d}\mathbf{y} \\
&= \int_B \int_{\mathbb{R}^n} r(\mathbf{q}) \pi_{Q^f,Y^f}(\mathbf{q}, \mathbf{y}) \mathrm{d}\mathbf{q} \mathrm{d}\mathbf{y} \\
&= \mathbb{E} \left[r \circ Q^f \mathbf{1}_B(Y^f) \right] \\
&= \int_A r \circ Q^f \mathbb{P}(\mathrm{d}\omega).
\end{aligned} \tag{A.2}$$

Therefore, the RV $\phi_{r \circ Q^f}(Y^f)$ is identical to the conditional expectation $\mathbb{E} [r \circ Q^f | Y^f]$. ■

Appendix B. Orthogonal property of the conditional expectation.

Theorem B.1 (Orthogonal projection). Assume $\mathbb{E} [|r \circ Q^f|^2] < \infty$. Let $L_2(\sigma_{Y^f})$ be the collection of all random variables of type $g(Y^f)$, where $g : \mathbb{R}^m \rightarrow \mathbb{R}$ is an arbitrary function satisfying $\mathbb{E} [g(Y)^2] < \infty$. Then, A)

$$\mathbb{E} \left[g \circ Y^f \left(r \circ Q^f - \mathbb{E} [r \circ Q^f | Y^f] \right) \right] = 0, \tag{B.1}$$

B) the conditional expectation $\mathbb{E} [Q^f | Y^f]$ is the RV in $L_2(\sigma_{Y^f})$ that minimizes the MSE, i.e.,

$$\begin{aligned}
\mathbb{E} [r \circ Q^f | Y^f] &= \phi_{r \circ Q^f}(Y^f), \\
\text{where } \phi_{r \circ Q^f} &= \arg \min_{g \circ Y^f \in L_2(\sigma_{Y^f})} \mathbb{E} [|r \circ Q^f - g \circ Y^f|^2].
\end{aligned} \tag{B.2}$$

Proof. For any measurable set $B \subset \mathbb{R}^m$, let $A = Y^f - 1(B) \equiv \{\omega : Y^f(\omega) \in B\}$. As $A \in \sigma_{Y^f}$, we achieve

$$\begin{aligned}
\mathbb{E} \left[\mathbf{1}_B(Y^f) \left(r \circ Q^f - \mathbb{E} [r \circ Q^f | Y^f] \right) \right] &= \mathbb{E} \left[\mathbf{1}_B(Y^f) r \circ Q^f \right] - \mathbb{E} \left[\mathbf{1}_B(Y^f) \mathbb{E} [r \circ Q^f | Y^f] \right] \\
&= \int_A r \circ Q^f(\omega) \mathrm{d}\mathbb{P}(\omega) - \int_A \mathbb{E} [r \circ Q^f | Y^f](\omega) \mathrm{d}\mathbb{P}(\omega) \\
&= 0
\end{aligned} \tag{B.3}$$

Let X^n be a σ_{Y^f} -measurable simple RV that converges in terms of distribution to $g \circ Y^f$. Using the result from Eq. (B.3), we prove part A).

Let $Z = \mathbb{E} [r \circ Q^f | Y^f] - \phi_{r \circ Q^f}(Y^f)$, we have

$$\begin{aligned}
\mathbb{E} [|r \circ Q^f - \phi_{r \circ Q^f}(Y^f)|^2] &= \mathbb{E} [|r \circ Q^f - \mathbb{E} [r \circ Q^f | Y^f] + Z|^2] \\
&= \mathbb{E} [|r \circ Q^f - \mathbb{E} [r \circ Q^f | Y^f]|^2] + \mathbb{E} [|Z|^2],
\end{aligned} \tag{B.4}$$

as the cross-product term vanishes. Eq. (B.4) straightforwardly shows that $\mathbb{E} \left[|r \circ Q^f - \phi_{r \circ Q^f}(Y^f)|^2 \right]$ is minimized when $Z = 0$ or $\mathbb{E} [r \circ Q^f | Y^f] = \phi_{r \circ Q^f}(Y_f)$ (part B). ■

Appendix C. Proof of Lemma 3.1. The linear approximation of the CM, $g_l(Y^f) = \mathbf{A}Y^f + \mathbf{b}$, is the solution of the least mean square problem:

$$(C.1) \quad \mathbf{A}, \mathbf{b} = \arg \min_{\mathbf{A}' \in \mathbb{R}^{n \times m}, \mathbf{b}' \in \mathbb{R}^n} \mathbb{E} \left[\|Q^f - \mathbf{K}'Y^f - \mathbf{b}'\|^2 \right].$$

Using the first order necessary conditions

$$(C.2) \quad \mathbb{E} \left[Q^f - \mathbf{A}Y^f - \mathbf{b} \right] = \mathbf{0}_n,$$

and

$$(C.3) \quad \mathbb{E} \left[(Q^f - \mathbf{A}Y^f - \mathbf{b})Y^{f\top} \right] = \mathbf{0}_{n \times m},$$

where $\mathbf{0}_n$ and $\mathbf{0}_{n \times m}$ denote the n -dimensional vector and the $n \times m$ matrix of zeros repetitively. Thus, we obtain

$$(C.4) \quad \mathbf{b} = \mathbb{E} \left[Q^f - \mathbf{A}Y^f \right],$$

$$(C.5) \quad \begin{aligned} \mathbf{A} &= \mathbb{E} \left[(Q^f - \mathbb{E}[Q^f])Y^{f\top} \right] \mathbb{E} \left[(Y^f - \mathbb{E}[Y^f])Y^{f\top} \right]^{-1} \\ &= \mathbb{E} \left[(Q^f - \mathbb{E}[Q^f])(Y^f - \mathbb{E}[Y^f])^\top \right] \mathbb{E} \left[(Y^f - \mathbb{E}[Y^f])(Y^f - \mathbb{E}[Y^f])^\top \right]^{-1} \\ &= \text{Cov} \left[Q^f, Y^f \right] \text{Cov} \left[Y^f \right]^{-1}. \end{aligned}$$

In conclusion, \mathbf{A} is identical to the Kalman gain defined in Eq. (3.9).

REFERENCES

- [1] H. D. ABARBANEL, P. J. ROZDEBA, AND S. SHIRMAN, *Machine learning: deepest learning as statistical data assimilation problems*, Neural Computation, 30 (2018), pp. 2025–2055.
- [2] M. ADES AND P. J. VAN LEEUWEN, *An exploration of the equivalent weights particle filter*, Quarterly Journal of the Royal Meteorological Society, 139 (2013), pp. 820–840.
- [3] S.-I. AMARI, *Backpropagation and stochastic gradient descent method*, Neurocomputing, 5 (1993), pp. 185–196.
- [4] M. ASCH, M. BOCQUET, AND M. NODET, *Data assimilation: methods, algorithms, and applications*, SIAM, 2016.
- [5] P. BAUER, B. STEVENS, AND W. HAZELEGER, *A digital twin of earth for the green transition*, Nature Climate Change, 11 (2021), pp. 80–83.
- [6] A. BOBROWSKI, *Functional analysis for Probability and Stochastic Process*, Cambridge University press, 2005.
- [7] M. BOCQUET, J. BRAJARD, A. CARRASSI, AND L. BERTINO, *Bayesian inference of chaotic dynamics by merging data assimilation, machine learning and expectation-maximization*, Foundations of Data Science, 2 (2020), p. 55.

- [8] J. BRAJARD, A. CARASSI, M. BOCQUET, AND L. BERTINO, *Combining data assimilation and machine learning to emulate a dynamical model from sparse and noisy observations: a case study with the Lorenz 96 model*, arXiv preprint arXiv:2001.01520, (2020).
- [9] F. BURDEN AND D. WINKLER, *Bayesian regularization of neural networks*, Artificial Neural Networks, (2008), pp. 23–42.
- [10] R. DURRETT, *Probability: theory and examples*, vol. 49, Cambridge University press, 2019.
- [11] O. G. ERNST, B. SPRUNGK, AND H.-J. STARKLOFF, *Bayesian inverse problems and Kalman filters*, in Extraction of Quantifiable Information from Complex Systems, Springer, 2014, pp. 133–159.
- [12] G. EVENSEN, *Data assimilation: The ensemble Kalman filter*, Springer Berlin Heidelberg, 2009.
- [13] D. J. GAGNE, H. M. CHRISTENSEN, A. C. SUBRAMANIAN, AND A. H. MONAHAN, *Machine learning for stochastic parameterization: generative adversarial networks in the Lorenz 96 model*, Journal of Advances in Modeling Earth Systems, 12 (2020), p. e2019MS001896.
- [14] I. GOODFELLOW, Y. BENGIO, A. COURVILLE, AND Y. BENGIO, *Deep learning*, vol. 1, MIT press Cambridge, 2016.
- [15] H. HOEL, K. J. H. LAW, AND R. TEMPONE, *Multilevel ensemble Kalman filtering*, SIAM Journal on Numerical Analysis, 54 (2016), pp. 1813–1839.
- [16] P. L. HOUTEKAMER AND H. L. MITCHELL, *Data assimilation using an ensemble Kalman filter technique*, Monthly Weather Review, 126 (1998), pp. 796–811.
- [17] R. E. KALMAN, *A new approach to linear filtering and prediction problems*, Transactions of the ASME Journal of Basic Engineering, 82 (1960), pp. 35–45.
- [18] D. P. KINGMA AND J. BA, *Adam: a method for stochastic optimization*, arXiv preprint arXiv:1412.6980, (2014).
- [19] K. J. H. LAW, A. STUART, AND K. ZYGALAKIS, *Data assimilation*, Cham, Switzerland: Springer, 214 (2015).
- [20] K. J. H. LAW, H. TEMBINE, AND R. TEMPONE, *Deterministic mean-field ensemble Kalman filtering*, SIAM Journal on Scientific Computing, 38 (2016), pp. A1251–A1279.
- [21] Y. LEE AND A. J. MAJDA, *State estimation and prediction using clustered particle filters*, Proceedings of the National Academy of Sciences, 113 (2016), pp. 14609–14614.
- [22] J. LEI AND P. BICKEL, *A moment matching ensemble filter for nonlinear non-Gaussian data assimilation*, Monthly Weather Review, 139 (2011), pp. 3964–3973.
- [23] E. N. LORENZ, *Deterministic nonperiodic flow*, Journal of Atmospheric Sciences, 20 (1963), pp. 130–141.
- [24] E. N. LORENZ, *Predictability: A problem partly solved*, in Proc. Seminar on Predictability, vol. 1, 1996.
- [25] E. N. LORENZ AND K. A. EMANUEL, *Optimal sites for supplementary weather observations: simulation with a small model*, Journal of the Atmospheric Sciences, 55 (1998), pp. 399–414.
- [26] A. J. MAJDA AND J. HARLIM, *Filtering complex turbulent systems*, Cambridge University Press, 2012.
- [27] H. G. MATTHIES, E. ZANDER, B. V. ROSIĆ, AND A. LITVINENKO, *Parameter estimation via conditional expectation: a Bayesian inversion*, Advanced modeling and simulation in engineering sciences, 3 (2016), pp. 1–21.
- [28] A. RASHEED, O. SAN, AND T. KVAMSDAL, *Digital twin: values, challenges and enablers from a modeling perspective*, IEEE Access, 8 (2020), pp. 21980–22012.
- [29] R. H. REICHLE, *Data assimilation methods in the earth sciences*, Advances in water resources, 31 (2008), pp. 1411–1418.
- [30] A. SPANTINI, R. BAPTISTA, AND Y. MARZOUK, *Coupling techniques for nonlinear ensemble filtering*, arXiv preprint arXiv:1907.00389, (2019).
- [31] M. VERLAAN AND A. W. HEEMINK, *Nonlinearity in data assimilation applications: a practical method for analysis*, Monthly Weather Review, 129 (2001), pp. 1578–1589.
- [32] J. VONDREJC AND H. G. MATTHIES, *Accurate computation of conditional expectation for highly nonlinear problems*, SIAM/ASA Journal on Uncertainty Quantification, 7 (2019), pp. 1349–1368.